Geophysical Research Letters

Supporting Information for

Fate of the Atlantic Meridional Overturning Circulation – Strong decline under continued warming and Greenland melting

P. Bakker[1†], A. Schmittner[1], J.T.M. Lenaerts[2], A. Abe-Ouchi[3], D. Bi[4], M.R. van den Broeke[2], W-L. Chan[3], A. Hu[5], R. L. Beadling[6], S.J. Marsland[4], S.H. Mernild[7,8], O.A. Saenko[9], D. Swingedouw[10], A. Sullivan[4], and J. Yin[6]

[1] Oregon State University, USA
[2] Institute for Marine and Atmospheric research, Utrecht University, Netherlands
[3] Atmosphere and Ocean Research Institute, University of Tokyo, Japan
[4] CSIRO Oceans and Atmosphere, Australia
[5] National Center for Atmospheric Research, USA
[6] University of Arizona, USA
[7] Sogn og Fjordane University College, Sogndal, Norway
[8] Antarctic and Sub-Antarctic Program, Universidad de Magallanes, Punta Arenas, Chile
[9] Canadian Centre for Climate Modelling and Analysis, Canada
[10] Institut Pierre-Simon Laplace, France
† Now at MARUM, Bremen University, Germany

Contents of this file

Introduction

In this Supporting Information we provide a more detailed description of the main methods of the manuscript, relating to the GrIS meltwater forcing, the AMOC-emulator and the uncertainty analyses. Furthermore, we present in Figures 1-3 the fit of the AMOC-emulator to the individual GCM simulations, the regional temperature forcings and GrIS melt forcing applied in the probabilistic AMOC projections. In figure 4 the quantification of the uncertainty introduced by the AMOC-emulator is shown and in figure 5 the impact of calving on AMOC change probabilities as a function of global temperature change. In Table 1 we provide an overview of the participating models in AMOCMIP and model details on the performed simulations and in table 2 an overview of the results of the probabilistic AMOC projections for different combinations of temperature changes, GrIS melt and calving.

Text S1: Methodology

GrIS meltwater forcing

We calculate GrIS meltwater fluxes following [*Lenaerts et al.*, 2015], who find a strong relation between mid-tropospheric (500hPa) summer (June-July-August) temperature changes over the GrIS and annual GrIS runoff analyzing high-resolution regional climate model simulations. Second-order polynomials were based on a high resolution (~11km) RACMO2 regional climate model simulation for the period 1971-2100, forced at the boundaries by HadGEM2-ES GCM output under the RCP4.5 scenario [*Lenaerts et al.*, 2015]. Strong spatial variations in GrIS runoff are included by performing these calculations separately for eight glacial sections of the GrIS [*Wouters et al.*, 2008]. A fixed seasonal GrIS runoff cycle is imposed based on a scaling of the average RACMO2 seasonal cycle for the period 1960-2012.

To derive GrIS mass loss projections for AMOCMIP, CMIP5 multi-model-mean (MMM) 500hPa summer temperature anomalies are calculated from all available RCP4.5 and RCP8.5 simulations that cover (part of) the period 2006-2300. Because of data availability, the MMM 500hPa summer temperature anomalies consist of 39 to as little as 5 model simulations for individual scenarios and time intervals. Temperature anomalies are calculated with respect to the GCM's historical average 1971-2000 temperatures. If multiple ensemble members exist only the first or longest member was used. The differences in the number of simulations that is included in the MMM result in spurious shifts in both the mean and inter-model spread, however, those are small compared to the overall signal. The GrIS runoff parameterization includes changes in precipitation, evaporation, snow and ice melt, and meltwater refreezing and retention in the snow-pack [*Lenaerts et al.*, 2015]. The high complexity and resolution of RACMO2 compared to GCMs ensures a much better representation of real-world atmospheric and snow processes and topography. In order not to double count the impact on GrIS runoff of changes in precipitation, evaporation and snow melt, GrIS runoff changes calculated by the GCMs are neglected. The way the freshwater forcing is added to the ocean differes per GCM and is listed in Table SI1.

The above-described GrIS mass loss projections are added to two different historical GrIS runoff 'baselines': the amount of historical GrIS runoff including a spatial pattern and a seasonal cycle. The first baseline (gGrISmelt) is an 1971-2000 average for the individual GCMs including the GCMs GrIS runoff seasonal cycle. The total GrIS runoff (baseline+melt projection) thus differs somewhat between the GCMs in the gGrISmelt experiments because the baseline is different for each GCM. The second baseline (rGrISmelt) is constructed in order to have the most realistic GrIS runoff baseline. It includes average RACMO2-based historical (1971-2000) liquid runoff for the eight GrIS drainage basins including the RACMO2-based seasonal cycle. In addition, it includes the annual mean total observed GrIS solid ice calving rate [*Enderlin et al.*, 2014] that is spatially distributed over the North Atlantic and Arctic based on high-resolution ocean-ice-berg simulation of [*Berk and Drijfhout*, 2014]. Simulating the two different GrIS runoff baselines allows us to assess the importance of its uncertainty. The projected GrIS mass loss is equally distributed over the coastal cells corresponding to the eight glacial GrIS sections [*Wouters et al.*, 2008] following *Lenaerts et al.* [2015]. The

gGrISmelt baseline flux is equally distributed over all coastal grid cells, as is the liquid runoff part of the rGrISmelt basineline, while the solid ice calving part of the rGrISmelt basineline follows the spatial distribution that was simulated by *Berk and Drijfhout* [2014]. For three models (CCSM4, CESM1.1.2 and MIROC4m) the applied GrIS meltwater forcing differs somewhat from the AMOCMIP protocol. In CCSM4 the total GrIS meltwater fluxes are larger by 13%, 6%, 28% and 18% averaged over the whole simulated period for respectively the RCP4.5-gGrISmelt, RCP4.5-rGrISmelt, RCP8.5-gGrISmelt and RCP8.5-rGrISmelt. Similarly, in MIROC4m the GrIS meltwater fluxes are larger by <5%. In both cases this is because GCM-based GrIS runoff changes were included while they should have been neglected. The applied GrIS meltwater anomalies in CESM1.1.2 are smaller than in the AMOCMIP protocol, by 11% averaged over the whole simulated period for RCP8.5-gGrISmelt. This is because GrIS mass loss projections in the CESM1.1.2 simulation was based on CESM1.1.2 500hPa summer temperature changes [*Lenaerts et al.*, 2015] rather than MMM values. The impact on the results is likely small since the impact of GrIS mass loss on the AMOC evolution in these models is small. Importantly, the use of the AMOC-emulator allows us to correct for the GrIS meltwater forcing differences in the final probabilistic AMOC projections.

Not considered in the GrIS mass loss projections used in the GCMs are changes in solid ice discharge (ice-berg calving). Presently, the constraints on the sign and magnitude of GrIS solid-ice discharge projections are insufficient to be included in the AMOCMIP forcing [*Lenaerts et al.*, 2015; *Nick et al.*, 2009]. However, we have used the AMOC-emulator to assess the possible impact of future changes in solid ice discharge. We impose idealized ±1% changes per year, capped when the flux doubles or becomes zero (after ~70yrs). The results of these experiments are compared with the results of the AMOC-emulator simulations that exclude changes in solid ice discharge in Table SI2.

AMOC-emulator

The AMOC-emulator used here is a four-box model that uses physical and dynamicsl relationships to represent the most important mechanisms and feedbacks that govern the AMOC's response to changes in surface temperatures and freshwater input [*Bakker and Schmittner*, 2016]. It is an adjusted version of a previously published AMOC box model [*Stommel*, 1961; *Zickfeld et al.*, 2004], coupled to a 1D atmospheric energy balance model to include the first-order feedback from the atmosphere on AMOC changes, the so-called Bjerknes feedback [*Rahmstorf and Willebrand*, 1995]. It describes the AMOC strength as a linear function of the density contrast between the North Atlantic and the South Atlantic [*Stommel*, 1961]. Changes in freshwater transport between the South Atlantic and the Equatorial box, and between the Equatorial box and the North Atlantic is parameterized as a linear function of global temperature changes [*Zickfeld et al.*, 2004], including a free parameter that is part of the AMOC-emulator tuning. The AMOC emulator can reproduce the behavior of a specific GCM by tuning a number of free parameters such that the difference between the AMOC's response in the GCM and the AMOC-emulator to a given set of changes in boundary conditions is minimized. Simulated Annealing is used for the parameter estimation [*Lombardi*, 2015], a stochastic method to solve problems of

multidimensional global optimization that is able to escape from local minima or maxima. The tuning of the AMOC-emulators for the different GCM's is based on all performed AMOCMIP experiments and corresponding standard RCP scenarios. The amount of tuning data thus differs per GCM. An extensive description of the AMOC-emulator, the free parameters, tuning procedure and GCM-based AMOC-emulator forcings as well as an evaluation of the predictive power of the AMOC-emulator can be found elsewhere [*Bakker and Schmittner*, 2016].

Uncertainty analysis

Five types of uncertainty are included in the probabilistic AMOC projections: GHG concentration changes, AMOC sensitivity to climate and GrIS meltwater forcing, climate sensitivity to GHG forcing, regional temperature changes and GrIS mass loss. GHG concentration changes are considered by using two different RCP scenarios (RCP4.5, and RCP8.5). The other uncertainties are included using a Monte-Carlo approach with a total of n=10,000 samples per RCP scenario and set of forcings. The uncertainty in the AMOC's sensitivity to changes in regional temperatures and freshwater budgets is included by randomly picking an AMOC-emulator parameter-set that is tuned towards one of the participating GCMs. Furthermore, the parameter tuning procedure is repeated until for every GCM a total of 100 reasonable AMOC-emulators are found, of which the ten best (based on the squared distance between the AMOC in a GCM and in the AMOC-emulator [*Bakker and Schmittner*, 2016]) are included in the Monte-Carlo sampling. The uncertainty in climate sensitivity and regional temperature changes is treated simultaneously by semi-random sampling of CMIP5-based multi-model regional and global temperature change distributions for the period 2006-2300. An array T of n-samples for the whole time period 2006-2300 (length t) are taken for every region r assuming a Gaussian CMIP5-based temperature distribution:

$$T(r,t)=N(\mu(r,t),\sigma(r,t))$$

where μ and σ are the CMIP5-based temperature anomaly mean and standard deviations (relative to 2006) for the different regions: global, the five regions based on the latitude bands of the AMOC-emulator [*Bakker and Schmittner*, 2016] and a Greenland average. Note that the Greenland temperatures are summer 500hPa temperature anomalies used to calculate GrIS mass loss. Moreover, the random samples that are taken are a function of the region r, but are constant over time. To take into account the degree of spatial temperature change correlation that exists in GCMs, we calculate the region-to-region temperature correlation factors based on average temperatures over the last 10 years of the individual CMIP5 simulations for RCP4.5 and RCP8.5 and impose these correlations on the matrix T by multiplying it with the Cholesky decomposition of the CMIP5-based correlation factors. This procedure captures uncertainties in climate sensitivity, polar amplification and regional temperature change differences while maintaining a realistic degree of regional correlation. The temperature range sampled with matrix T is shown in Fig. SI2. The final uncertainty that is included in the probabilistic AMOC projections is the uncertainty in future GrIS mass loss. Following [*Lenaerts et al.*, 2015] annual mean GrIS runoff is derived from a second-order polynomial relation with summer 500hPa temperature anomalies over the eight GrIS drainage basins. The GrIS runoff uncertainty is included by a

combination of 1) the semi-random sampling of the summer 500hPa temperature changes over Greenland as described above (note that in the forcing of the AMOC-emulator we use CMIP5-based temperature anomalies over the whole of Greenland rather than the eight drainage basins because the differences are small on the relatively coarse GCM grids), and 2) a random sampling of the uncertainty in the calculated 2-order polynomial relations derived by recalculating them on random 95% subsamples of the original data [*Lenaerts et al.*, 2015]. The sampled range of GrIS mass loss is shown in Fig. SI3.

A final source of uncertainty in the presented probabilistic AMOC projections is the error introduced by using an AMOC-emulator, a highly simplified AMOC model, to resemble the complex behavior of fully coupled global climate models. It is not straightforward to determine the error that the AMOC-emulator makes since the purpose of using an emulator is to provide AMOC projections for GCM simulations that have not been performed. We include a first-order approximation of the AMOC-emulator induced uncertainty based on the GCM-emulator differences for those simulations that are available (Fig. SI1). We combine timeseries of the GCM-emulator differences for all available GCMs, scenario and AMOC-emulators (thin colored lines in Fig. SI4). For this this wealth of data, we calculate the overall mean and standard deviation (thick black and blue lines in Fig. SI4, respectively), which in turn we approximate by linear fits (thin red lines in Fig. SI4) in order not smooth out any short term variability. The final AMOC-emulator induced uncertainty is added to the AMOC projections by adding the mean±1 standard deviation to every AMOC-emulator run. In short, this results in applying a small bias correction that ranges from -0.288Sv at 2006 to 0.813Sv at 2300, and widening the uncertainty envelope by adding a standard deviation that ranges from 0.951Sv at 2006 to 2.560Sv at 2300. The large increase with time of the standard deviation of the GCM to AMOC-emulator differences resembles the increase of uncertainty with the length of the projection period.

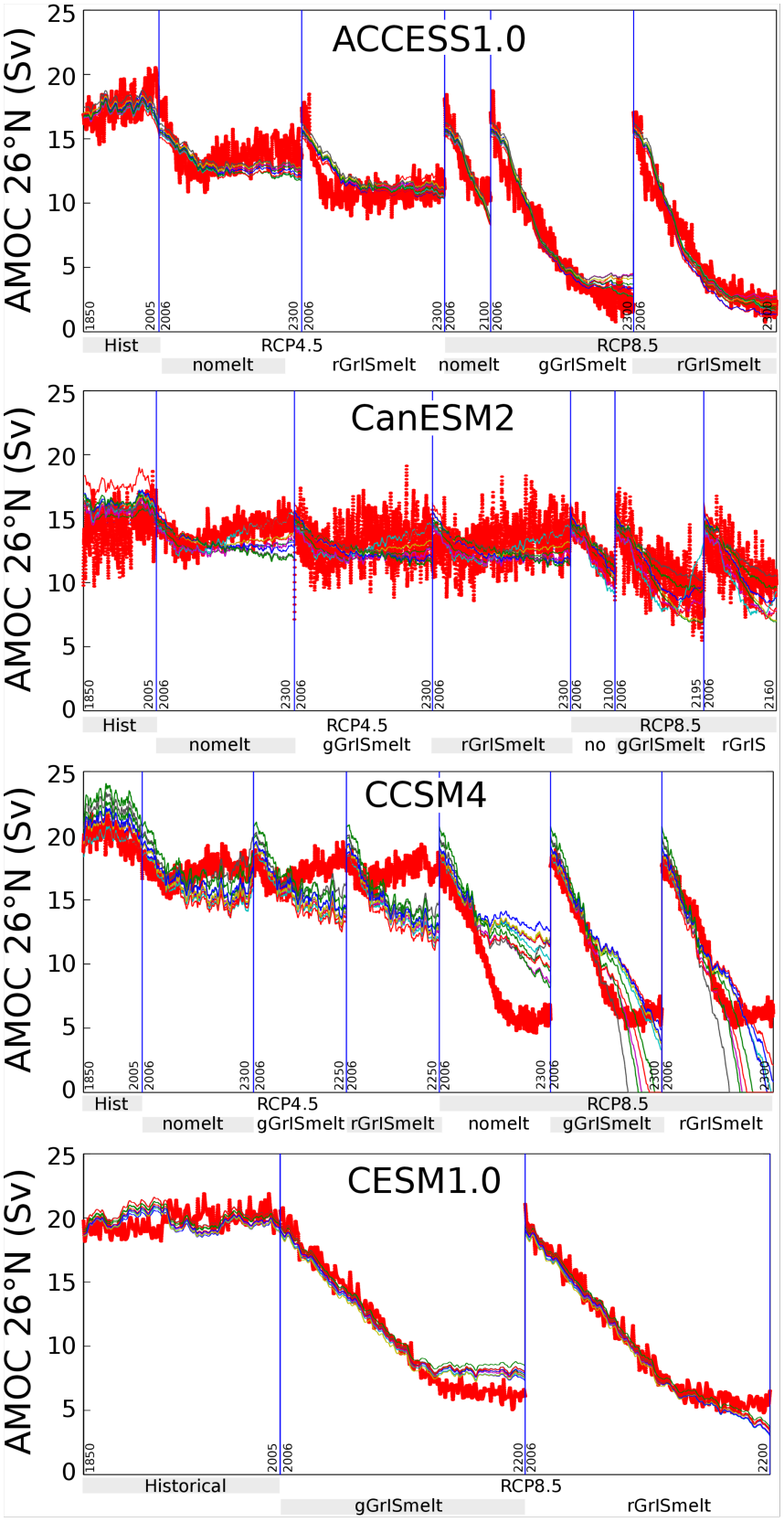
ACCESS1.0
AMOC 26°N (Sv)
25
20
15
10
5
0
1850
2005
2006
2300
2006
2300
2006
2100
2006
2300
2006
2300
Hist
RCP4.5
RCP8.5
nomelt
rGrlSmelt
nomelt
gGrlSmelt
rGrlSmelt
CanESM2
AMOC 26°N (Sv)
1850
2005
2006
2300
2006
2300
2006
2300
2006
2100
2006
2195
2006
2160
Hist
RCP4.5
RCP8.5
nomelt
gGrlSmelt
rGrlSmelt
no
gGrlSmelt
rGrlS
CCSM4
AMOC 26°N (Sv)
1850
2005
2006
2300
2006
2250
2006
2250
2006
2300
2006
2300
2006
2300
Hist
RCP4.5
RCP8.5
nomelt
gGrlSmelt
rGrlSmelt
nomelt
gGrlSmelt
rGrlSmelt
CESM1.0
AMOC 26°N (Sv)
1850
2005
2006
2200
2006
2200
Historical
RCP8.5
gGrlSmelt
rGrlSmelt

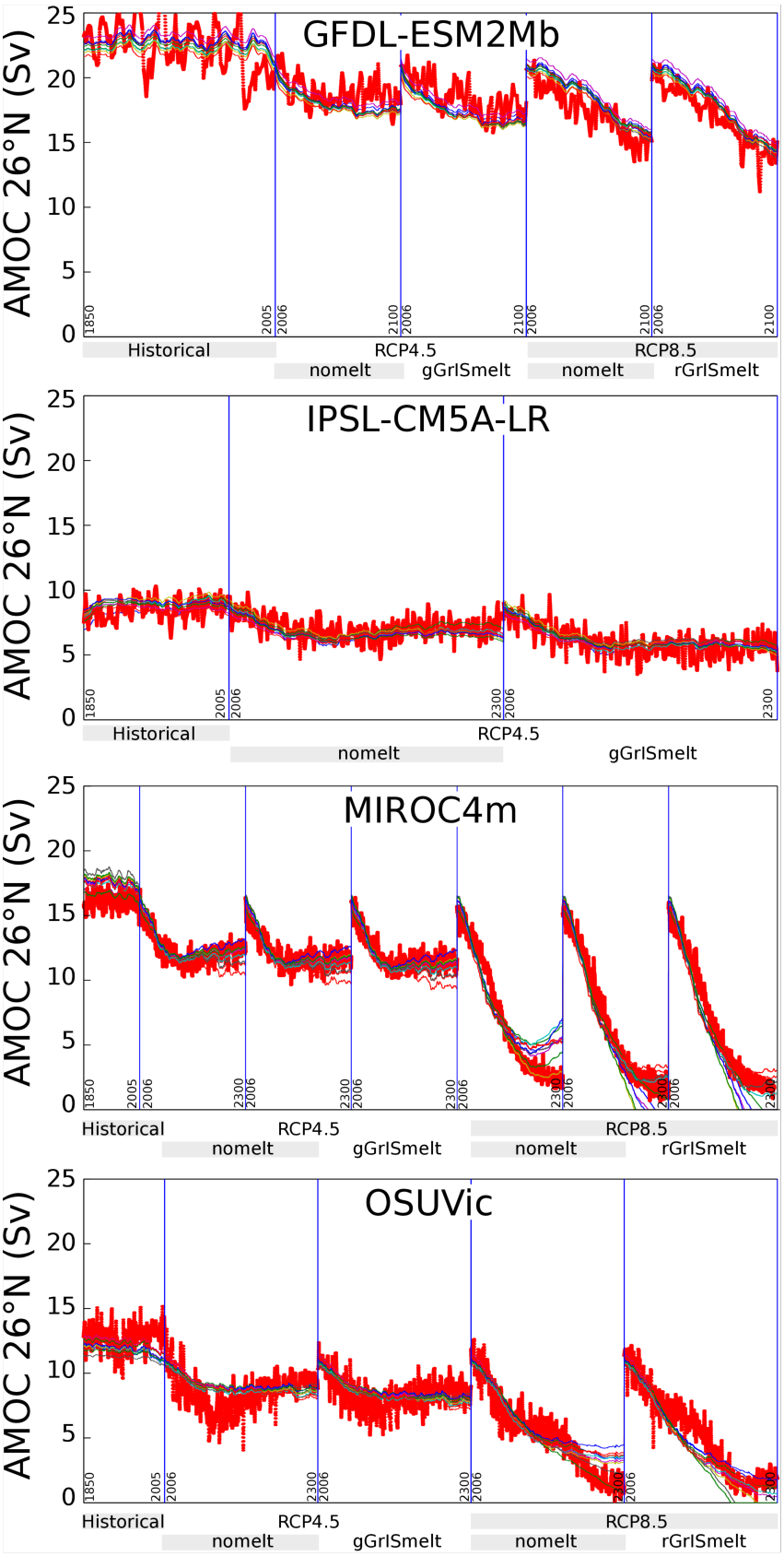
GFDL-ESM2Mb
IPSL-CM5A-LR
MIROC4m
OSUVic
AMOC 26°N (Sv)
0
5
10
15
20
25
1850
2005
2006
2100
2300
Historical
RCP4.5
RCP8.5
nomelt
gGrlSmelt
rGrlSmelt

Figure SI1. AMOC-emulator fits to AMOC simulated by individual GCMs. For participating AMOCMIP GCMs all AMOC strength at 26°N output (Sv; thick red lines) that is used in the AMOC-emulator tuning process is shown for all scenarios (pasted one after the other). Thin colored lines show the 10-best fitting AMOC emulators (out of a 100 reasonable) for every individual GCM that are used in the probabilistic AMOC projections. The maximum overturning stream function in the Atlantic at 26°N below 500m depth is taken as a measure of the AMOC strength.

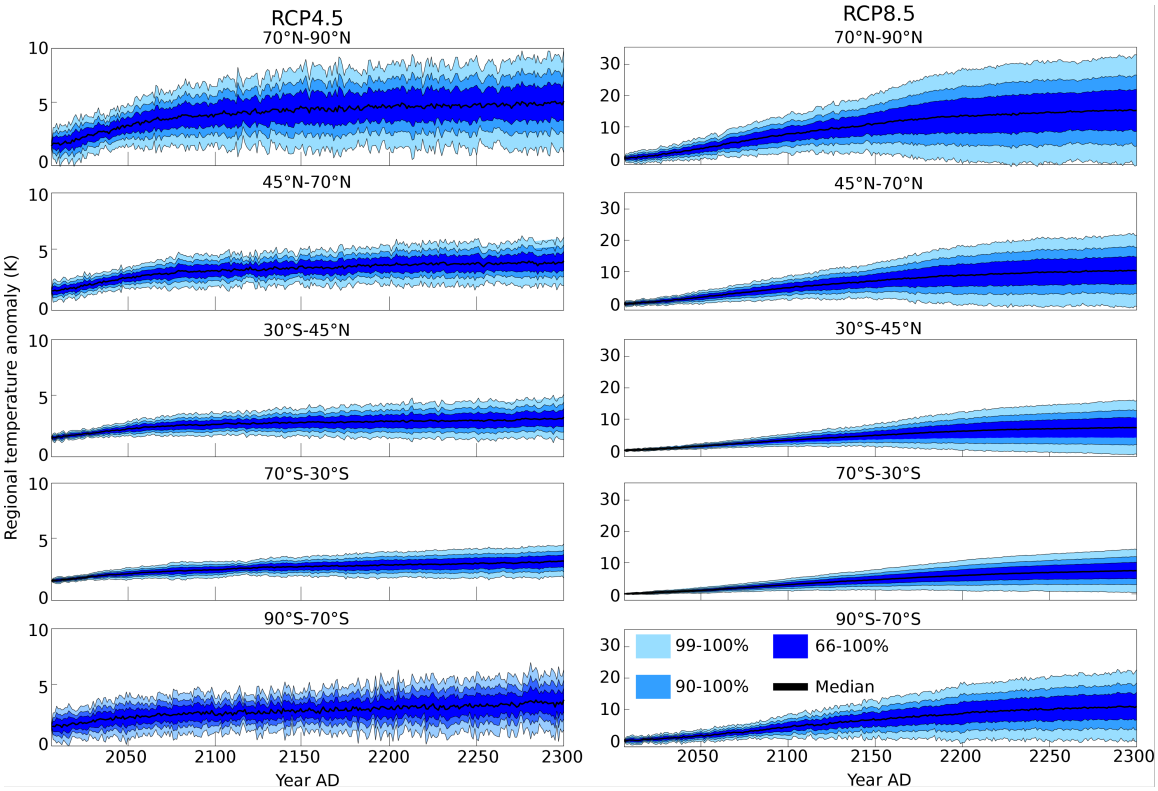

240 ***Figure SI2.*** *CMIP5-based regional temperature evolution distributions for RCP4.5 and RCP8.5 used in the probabilistic AMOC evolution assessment. Note that these distributions are sampled semi-randomly because CMIP5-based inter-regional temperature change correlations are imposed through Cholesky decomposition of the correlation factors.*

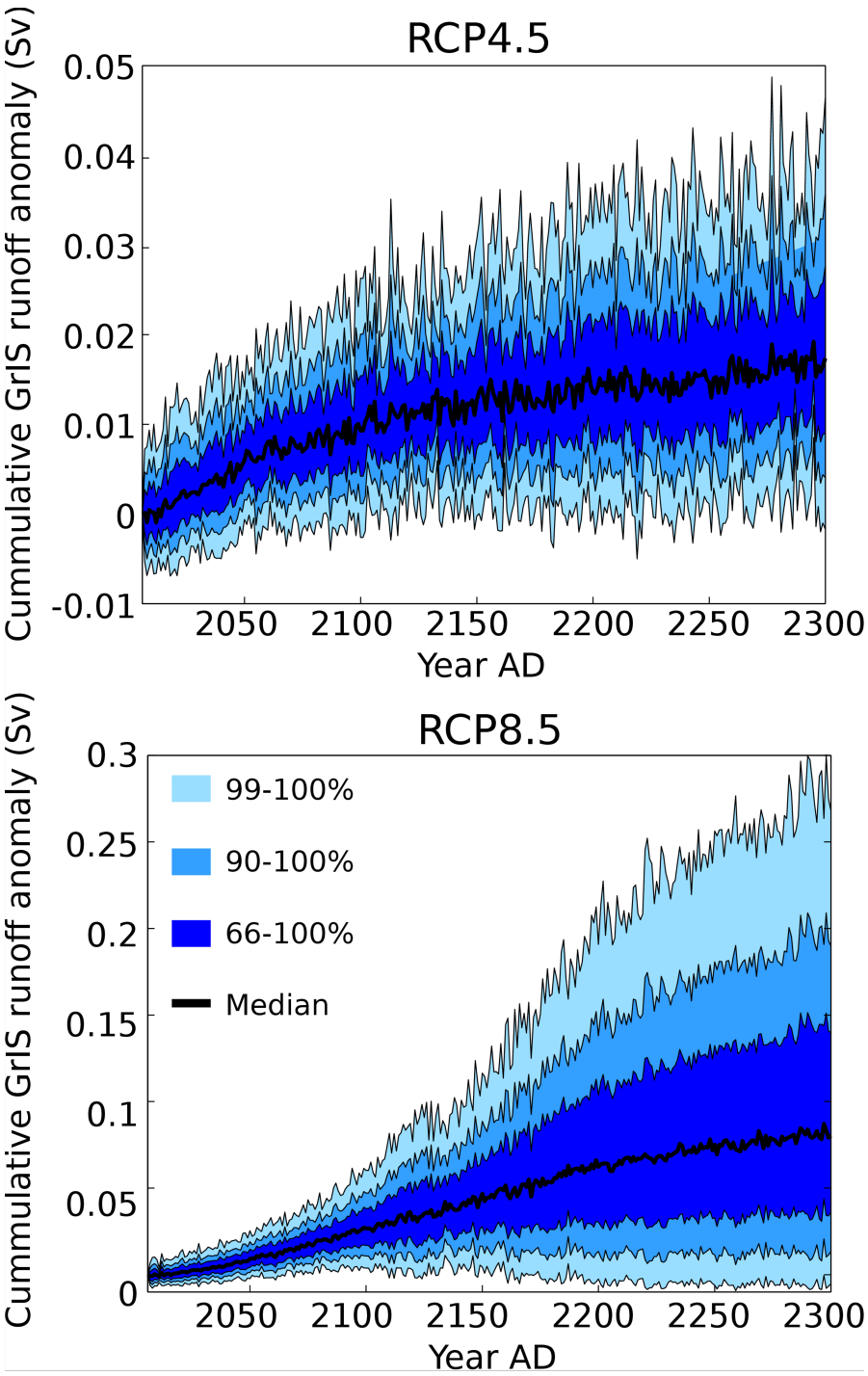

Figure SI3. *GrIS meltwater evolution distributions for RCP4.5 and RCP8.5 used in the probabilistic AMOC evolution assessment.*

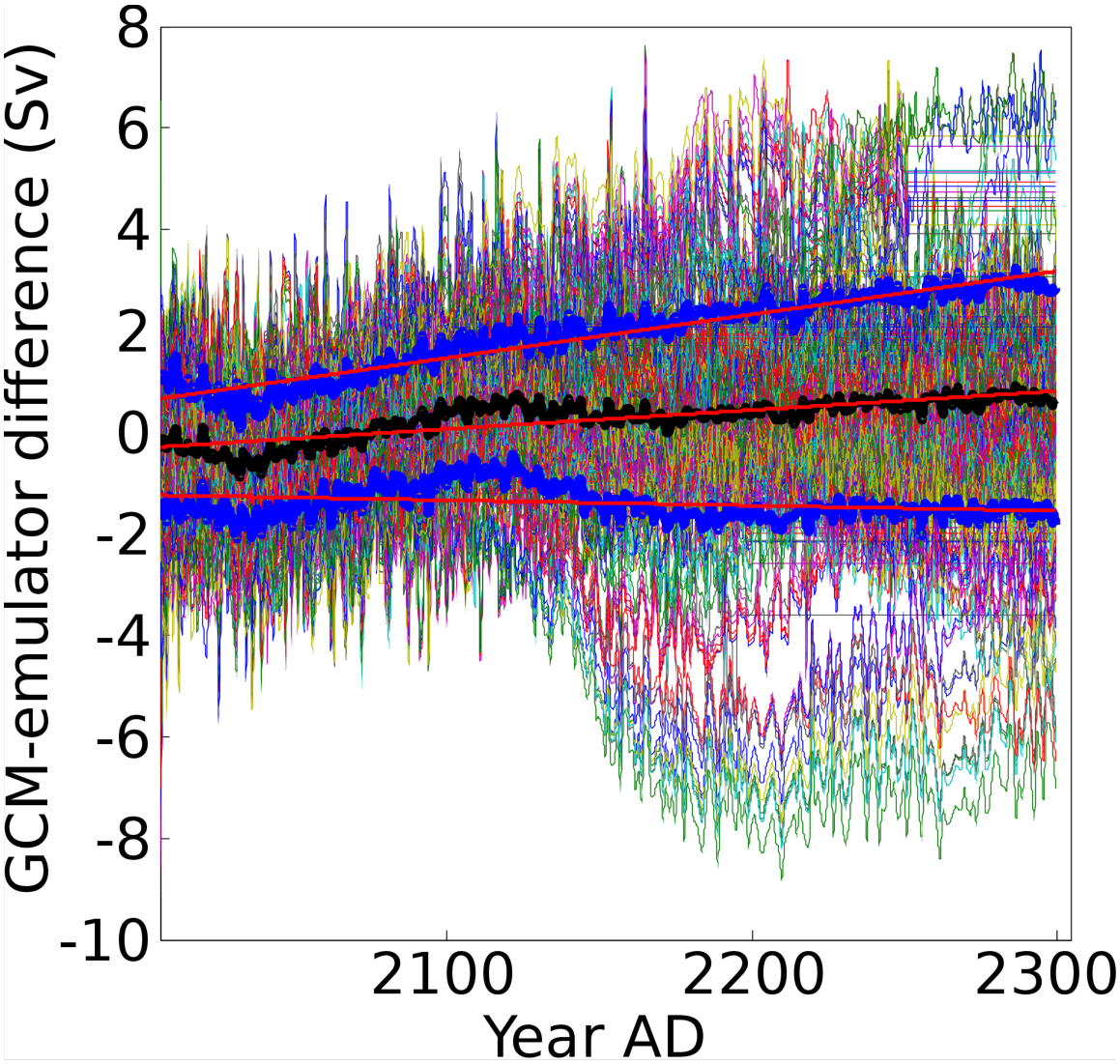

Figure SI4. *Quantification of the uncertainty induced by the AMOC-emulator. Shown are GCM to AMOC-emulator differences (GCM minus emulator) for all GCMs, RCP-scenarios, forcing scenarios and AMOC-emulators for which GCM results are available for at least part of the 2006-2300 year period (think colored lines). The mean and mean ± standard deviation are shown in thick black and blue lines, respectively. Thin red lines show linear fits to the mean and standard deviations that are used to quantify the uncertainty induced by the AMOC-emulator in the AMOC projections. Note that if GCM results are only available for part of the 2006-2300 year period, a constant value is assumed for the remainder of the period based on an average over the last 10 years for which GCM results are available, thus the resulting flat lines in for instance the upper right corner.*

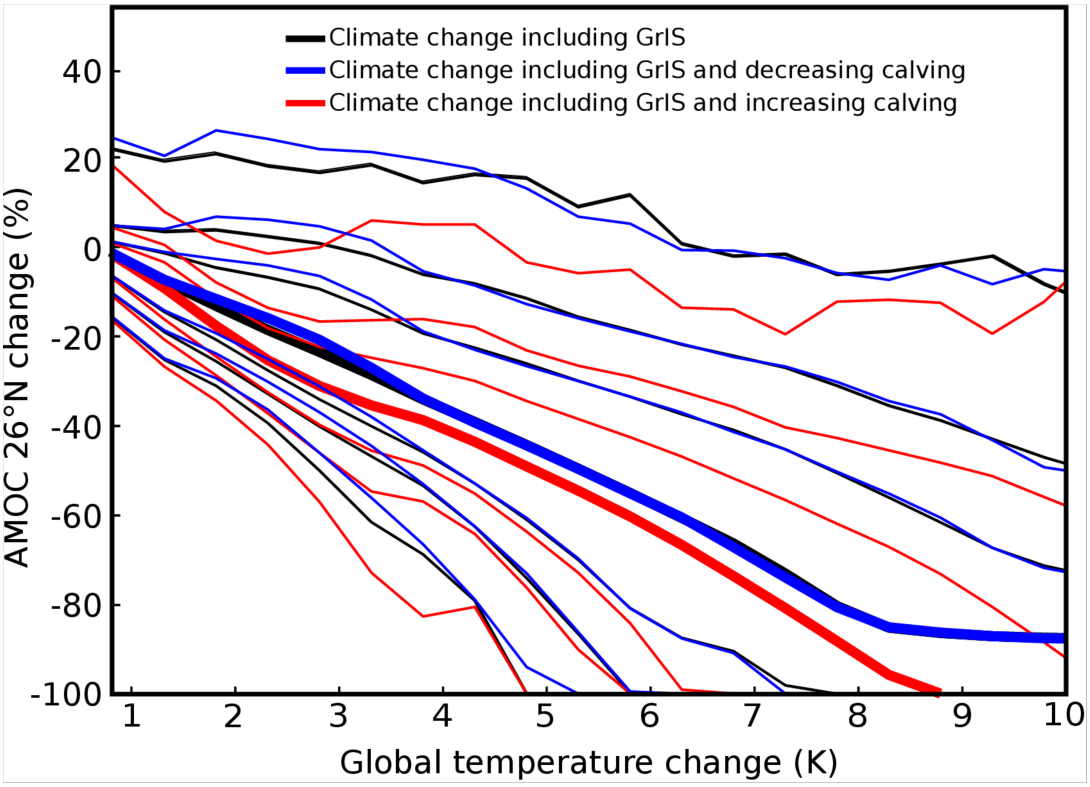

Figure SI5. *Impact of uncertainty in the evolution of GrIS calving rates on the probability of AMOC strength changes as a function of global temperature changes. Black lines (Climate change including GrIS) provides same information as in Fig. 3. Blue (red) gives results for 'Climate change including GrIS and de(in)creasing calving'. AMOC strength changes (%) are given at 26°N (below 500m; %) and global temperature change (K) are relative to pre-industrial. Thick lines show 5% probability, while the thin lines give (from top to bottom): 0.5%, 5%, 16.5%, 83.5%, 95% and 99.5% probability. For the 'Climate change including GrIS' scenario the likelihood of an AMOC collapse (defined here as a 90% weakening) is <1%, 11%, 19% and 30% for global temperature changes of 5K, 6K, 7K and 8K, respectively. For the 'Climate change including GrIS and decreasing calving' scenario, the likelihoods of an AMOC collapse are nearly identical. However, for the 'Climate change including GrIS and increasing calving', the likelihood is increased to 3%, 16%, 33% and 52% for global temperature changes of 5K, 6K, 7K and 8K, respectively.*

50

Model name	Historical	RCP4.5	RCP4.5-gGrISmelt	RCP4.5-rGrISmelt	RCP8.5	RCP8.5-gGrISmelt	RCP8.5-rGrISmelt	Freshwater forcing method	Ocean Resolution (latitude x longitude x vertical levels)	Atmospheric Resolution (latitude x longitude x vertical levels)	Reference
ACCESS1.0	2006	2300		2300	2100	2300	2300	Freshwater	1x1x50levs	1.875x1.25x38levs	Dix et al., 2013
CanESM2	2006	2300	2300	2300	2100	2195	2160	Negative salt flux	1.41× 0.94x40levs	T63x35levs	Yang and Saenko, 2012
CCSM4	2006	2300	2250	2250	2300	2300	2300	Negative salt flux	1.11x0.27-0.54x60	0.9×1.25x26levs	Meehl et al., 2012
CESM1.1.2	2006				2200	2200		Negative salt flux	1.11x0.27-0.54x60	0.9×1.25x30levs	Meehl et al., 2013
GFDL-ESM2Mb	2006	2100	2100		2100	2100		Freshwater	1x(1-1/3)x50levs	2x2.5x24levs	Dunne et al., 2012
IPSL-CM5A-LR	2006	2300	2300					Freshwater	2x2x31levs	1.9x3.75x39levs	Dufresne et al., 2013
MIROC4m	2006	2300	2300	2300	2300	2300	2300	Freshwater	0.5-1.4x1.4x44levs	T42x20levs	Hasumi and Emori, 2004
OSUVic	2006	2300	2300	2300	2300	2300		Negative salt flux	1.8x3.6x19lev	T42x10levs	Schmittner et al., 2011

Table SI1. *AMOCMIP experimental and model overview. List of performed experiments given by the end-year and model details*

	2090-2100	2290-2300
RCP4.5		
Climate change including GrIS	-18 (-2 to -34)	-15 (+12 to -40)
Climate change excluding GrIS	-17 (-2 to -31)	-12 (+16 to -34)
GrIS only	-5 (+1 to -18)	-8 (+1 to -22)
Climate change including GrIS and decreasing calving	-16 (0 to -31)	-12 (+17 to -35)
Climate change including GrIS and increasing calving	-23 (-10 to -38)	-27 (-10 to -49)
RCP8.5		
Climate change including GrIS	-37 (-15 to -65)	-74 (+4 to -100)
Climate change excluding GrIS	-32 (-11 to -56)	-37 (+19 to -100)
GrIS only	-6 (0 to -20)	-21 (-5 to -61)
Climate change including GrIS and decreasing calving	-37 (-15 to -64)	-74 (+3 to -100)
Climate change including GrIS and increasing calving	-41 (-19 to -67)	-91 (-7 to -100)

Table SI2. *Overview of the probabilistic AMOC projections. Simulated AMOC changes (%; median and 90-100 probability ranges) are given for two time intervals (2090-2100 and 2290-2300) and for all performed experiments. For both RCP4.5 and RCP8.5 the results are listed for: climate change including GrIS melt, climate change excluding GrIS melt, GrIS melt only and the two additional experiments that test the impact of idealized ±1%yr^{-1} changes in GrIS solid ice discharge (decreasing and increasing calving).*